Wasit Journal of Engineering Sciences

Journal homepage: https://ejuow.uowasit.edu.iq

Numerical Investigation of the Impact of Subcooling Inlet on Water Flow Boiling Heat Transfer Through a Microchannel

Ahmed A. Y. Al-Waaly[1]

Affiliations
[1] Mechanical Engineering Department,
College of Engineering,
Wasit University,
Wasit, Iraq

Correspondence
Ahmed A. Y. Al-Waaly
aalwaaly@uowasit.edu.iq

Received
12-February-2024
Revised
26-February-2024
Accepted
04-March-2024

Doi:

Abstract

The effect of subcooling inlet has a big effect of the flow patterns for the flow boiling through a microchannel. Higher subcooling lower mass flux will delay the nucleate boiling and vice versa. The water flow boiling inside a microchannel has been analyzed numerically. The microchannel depth was 0.24 mm while the length was 40 mm. The supplied heat fluxes were 500 $kW \cdot m^{-2}$, 1000 $kW \cdot m^{-2}$and 1500 $kW \cdot m^{-2}$ with mass velocities of 400 $kg \cdot m^{-2} \cdot s^{-1}$ and 800 $kg \cdot m^{-2} \cdot s^{-1}$. The degrees of subcoooling of inlet water were 5ºC, 10ºC, 15ºC, 20ºC, and 25ºC. The results showed that the degree subcooling has a considerable impact on both the wall temperature and flow patterns. The rise in the degree of subcooling kept the nucleate flow boiling and retarded the development of convective boiling. In addition, there was a reflection point at which the impact of heat flux on the average of the convective coefficient of heat transfer was altered. The increase in the heat flux may lead to an increase or reduction in the average HTC with respect to the location of the reflection point. The reflection points were 7ºC and 5ºC for the mass velocities 400 $kg \cdot m^{-2} \cdot s^{-1}$ and 800 $kg \cdot m^{-2} \cdot s^{-1}$. Thus, both the degree of subcooling and the heat flux should be simultaneously considered when it comes to the enhancement of HTC during the flow boiling inside the microchannels.

Keywords: Water, Flow boiling, Nucleate boiling, Subcooling degree, Microchannel, CFD

الخلاصة:

تم تحليل تدفق الماء اثناء الغليان داخل قناة مايكروية عدديا. كان عمق القناة 0.24 ملم وطول القناة 40 مم^2. كانت قيمة الفيض الحراري المسلط 500 كيلو واط / م^2، 1000 كيلو واط / م^{2}و 1500 كيلو واط / م^2 بسرعات كتلية تبلغ 400 كجم/م^2 ث^1 و 800 كجم/م^2 ث^1. وكانت درجة حرارة التبريد الفائق للماع عند الدخول هي 5 °م، 10 °م، 15 °م، 20 °م، و25 °م. أظهرت النتائج أن درجة حرارة التبريد الفائق لدخول الماء لها تأثير كبير على كل من درجة حرارة الجدار وأنماط التدفق. أدى الارتفاع في درجة التبريد الفائق إلى إبقاء نمط الغليان ذو النوع النووي وتأخير تطور غليان الحمل الحراري. بالإضافة إلى ذلك، كانت هناك نقطة انقلاب تغير فيها تأثير الفيض الحراري على متوسط معامل الحمل الحراري لانتقال الحرارة. قد تؤدي الزيادة في الفيض الحراري إلى زيادة أو انخفاض في متوسط معامل الحمل الحراري فيما يتعلق بموقع نقطة الانقلاب. وكانت نقاط الانقلاب 7 °م و5 °م لسرعات الكتلة 400 كجم/م^2 ث^1 و800 كجم/م^2 ث^1 على التوالي. وبالتالي، ينبغي النظر في كل من درجة حرارة التبريد الفائق للماء والفيض الحراري في ان واحد عندما يتعلق الأمر بتعزيز معامل الحمل الحراري أثناء تدفق الغليان داخل القنوات المايكروية.

1. INTRODUCTION

The first using of microchannel has been adopted by the well-known article which was published by Tuckerman and Pease [1]. They constructed a compact heat sink by reducing the channel size by 1000 time into a microchannel to increase fluid-solid interaction area. They succeeded in their experiments to increase the amount of heat removed to 790 $W \cdot cm^{-2}$. The amount of heat removed by a single phase flow cooling through a microchannel can be improved by rising the pumping power. But, the more the increase in the heat generated on electronic devices, the more pumping power is required to dissipate the extra heat and reducing the temperature. This can be achieved by using

flow boiling in order to increase HTC which is in turn enhances the convection process and then reduces the high surface temperature [2-4].

Moreover, the flow boiling can enhance the cooling process over a small area and the pumping power required can be reduced [5] [6]. The flow boiling through a microchannel seems to be an excellent solution for cooling process of electronic circuits. But, there are some limitations to the use flow boiling in a microchannel for the cooling purposes such as the flow boiling instability [7].

Boiling is a process at which the phase is changed from liquid phase to vapour phase by heat addition. This relies on the bulk temperature level of the working fluid inside the microchannel, subcooled or saturated boiling. The saturated boiling is taking place if the liquid's bulk temperature is somewhat topmost than that of saturation condition while the flow boiling under subcooling inlet can be found when bulk liquid temperature below saturation temperature.

Lee and Mudawar [8] studied the influence of highly subcooling inlet during the flow boiling of refrigerant HFE 7100 through a microchannel on CHF, the bubble's detaching diameter, and void fraction. They concluded that the raising in heat flux leads to reduce bubble's detaching diameter and vapour void fraction and preventing the flow patterns transfers beyond the bubbly flow.

Ahmadi et al. [9] achieved an experimental work to exam the onset of nucleate boiling (ONB) for water. They studied the impact of pressure drop, subcooling inlet, mass velocity and heat flux on the flow boiling behaviour inside a stainless steel small tube with 6 mm outer's diameter and wall thickness 0.5mm. Their applied heat flux was between 40 $kW \cdot m^{-2}$ to 450 $kW \cdot m^{-2}$ and mass velocity range was from 70 $kg \cdot m^{-2} \cdot s^{-1}$ to 620 $kg \cdot m^{-2} \cdot s^{-1}$. Their results illustrated that the ONB's heat flux is highly dependent on the subcooling entry temperature, pressure, and mass velocity.

Le et al. [10] conducted a study to explore effect of subcooling effects on the flow boiling behaviour. They demonstrated that parameter that has the biggest effect is departure from nucleate boiling (DNB). They classified three types of flow with subcooling inlet: first type is bubbly flow which occurs with high mass velocity and high subcooling, the second type is vapour clots which is taking place under moderate subcooling, and the third type is slug flow which is observed at low mass velocity and near saturation. They suggested a new mechanism that triggering of DNB which is called concept. The assumed that at high local wall superheat, the dry creation can be controlled by nucleate bubbles, of near-wall vapour clots or vapour slug.
Sun et al. [11] explored the impact of microporous surfaces coating on water subcooled inlet flow boiling inside a small channel. They found that the rate of heat transfer will be reduced with the raising in mass velocity for the subcooled inlet. Moreover, compared to saturated boiling, the enhancement in HTC will be higher for subcooled inlet flow boiling. The change in the degree of subcooling from 30 ^oC to 70 ^oC, HTC will be raised from 84% to 173% in the subcooling region. While in the saturated region, the increase in HTC was will be from 178% to 202% and was independent on the subcooling degree.

Vafaei and Wen [12] performed an experimental work to exam the behaviour of water-alumina nanofluid during flow boiling of through a single stainless steel microchannel with 45 ^oC and 80 ^oC as a subcooling inlet. They concluded that the CHF increases remarkably with the very low nanoparticles concentrations. Moreover, the prevalent tendency of CHF of nanofluid shows a similar behaviour to that of pure water inside the microchannel.
Yin et al. [13] explored the influence of subcooling on sliding bubble during the departure from the wall. They tested the flow boiling of deionized water through a rectangular channel with cross-sectional dimensions 1 mm×1 mm. Their results confirmed that for a specific heat flux and subcooling inlet temperature, the increase in mass velocity will lead to advance in the onset of accelerated sliding (OAS). At specific mass velocity and inlet degree of subcooling, the OAS will be deferred with increase in low level of heat flux while OSA is going to be advanced when the heat flux approaches the high level.

Yin et al [14] evaluate the impact of the subcooling inlet on HTC and pressure drop inside a microchannel of large aspect ratio. The channel dimensions were 6mm in width, 0.3 mm in deep and the length was 40 mm and hydraulic diameter was 571μm. They concluded that at low Boiling number $Bo=2.9 \times 10^{-4}$, the nucleate flow boiling will be active because of high mass velocity and low heat flux. Whereas, the confined bubble flow was dominant when the boiling number around $Bo=5.0 \times 10^{-4}$. Moreover, the average HTC was depending on the applied heat flux than mass velocity, therefore, the nucleate boiling was dominant.

Lee and Mudawar [15] examined the impact of subcooling degree at the inlet on the flow boiling behaviour of refrigerant R-134a through 100 microchannel of length 609.5 mm and square cross section (1×1) mm^2. Their results showed that the subcooling zone is separated into PDB and FDB. Moreover, they confirmed that the saturated boiling is divided into three areas: nucleate boiling where vapour quality is 0.3, mixed between nucleate boiling and forced convective boiling for the vapour quality within the range 0.3 and 0.5, and then forced convective boiling for the quality above 0.5. At this point, the effect of dryout starts and leads to a reduction in HTC. The same conclusions are confirmed by Yeo and Lee [16]. They demonstrated that the subcooled inlet flow boiling can be

divided into two distinct sub-regions: PDB and FDB, and the transferring from PDB to FDB. Consequently, the HTC rapidly increases because of further bubbles are involving in the convection process.

Lee et al. [17] discussed experimentally the influence of high inlet subcooling on the flow behaviour for vertical upward flow of FC-72. The experimental setup consists of two-dimensional channel 5mm-146mm. The channel length consists of 114mm of heated length with wall thickness 1.05mm and 30 mm outlet (no-heated) length to avoid any outlet issues. Inlet subcooling temperature was 300.97 K, 304.54 K and 309.02 K. The authors used Lee model as a face change model which is effective in at estimation of phase change in the flow at any position for the flow boiling. Their results showed that the accuracy of estimation of the flow boiling behaviour reduces with the increase of mass velocity.

Chen et al. [18] studied a 3-dimensional conjugate heat transfer of the flow boiling through a minichannel with subcooling inlet. They demonstrated that during the flow boiling, the heat transfer mechanism starts with nucleate boiling and continues to vapour fraction of 0.45, and then the convective boiling will be dominant. The flow patterns start with bubbly flow which are growing, detaching and then coalescence. After the creation of some elongated bubbles, the raising in heat flux turns the flow into slug flow pattern. The local HTC rises with the raising in heat flux, and consequently, the vapour fraction raises up to 0.45. Moreover, the increasing in heat flux reduces the HTC where the vapour fraction becomes over 0.45 and dry batches are generated.

Jiang et al.[19] studied the impact of subcooling inlet of counter flow of multi-channel heat sink of the void fraction and flow stability. A heat sink with dimension 40mm×30mm with 25 channel, All the channels are diverging and converging, 13 of them in one direction while 12 in counter-flow direction. The length of each channel was 39.7 mm with 0.3 mm of the diverged outlet while the inlet 1.3mm and the channel depth was 3mm. De-ionized water was using as a working liquid. The inlet temperature was 50ºC, 60ºC, 70ºC, 80ºC, and 90ºC and different supplied heat fluxes and mass velocities were used. Their results confirmed that the design of counter flow diverging microchannel (CFDM) can achieve 140ºC wall temperature with heat flux 3525 $kW \cdot m^{-2}$in a large area 12 cm^2 with no sign of reaching the dryout. Moreover, a very low pressure drop was maintained with very high coefficient of performance.

There is a shortage of an inclusive conception of the flow behaviour inside the microchannel because of the complexity of the flow behaviour. Therefore, many studies attempted to analyze the flow boiling inside the microchannels using CFD [20]. CFD analysis is an effective tool to research the impact of different parameters on the flow boiling inside the microchannel such as: working fluid, geometry, mass velocity, and the applied heat flux. These parameters can effect on the rate of heat transfer, flow patterns, and the instability of the boiling process. In this work, a numerical analysis of water flow boiling inside a horizontal rectangular cross section microchannel is achieved. The effect of inlet degree of subcooling, heat flux, and mass velocity on water flow boiling is studied. Moreover, the effect of changing of average HTC during different flow patterns is extensively investigated.

2. MATHEMATICAL MODELING

The present model takes into account heat exchange between channel walls and flowing water which are represented by solid and fluid domains. Hence, transport equations for both domains are considered. For the solid domain, the conservation of energy equation accounts for the motion's heat transfer , heat transfer by conduction, and heat sources as follows [21]:

$$\frac{\partial(\rho_s H_s)}{\partial t}+\nabla\cdot\left(\rho_s U_s H_s\right)=\nabla\cdot(\lambda_s\cdot\nabla T_s)+S_{ES} \quad (1)$$

where H_s, ρ_s, λ_s, and T_s are the enthalpy, density, thermal conductivity, and temperature of the solid domain element, respectively. S_{ES} and U_s are the source terms of heat and motion, and ∇ is the gradient related to x, y and z directions. If the heat source term is ignored and the solid domain is stationary, the equation is reduced to

$$\frac{\partial(\rho_s H_s)}{\partial t}=\nabla\cdot\left(\lambda_s\cdot\nabla T_s\right) \quad (2)$$

For the fluid domain, the solution of CFD model is performed by instantaneous solving of the continuity, momentum, and thermal energy conservation transport equations. This allowed the determination of the flow variables such temperature, velocity, and energy of each element in the domain. For continuity and momentum, the homogenous multiphase flow approach was considered [21]. This model was based on the determination of mixture (bulk) transport properties using individual liquid and vapour phases. The continuity conservation transport equation is expressed by:

$$\frac{\partial\rho}{\partial t}+\nabla\cdot(\rho U)=S_c \quad (3)$$

where ρ is the bulk density and U is the velocity vector that are determined by:

$$\rho=\rho_v r_v+\rho_l(1-r_v) \tag{4}$$

and

$$U = U_v r_v+U_l(1-r_v) \tag{5}$$

where ρ_v, r_v, ρ_l, U_v, and U_l are vapour density, vapour void fraction, liquid density, vapour's velocity, and liquid's velocity respectively. The term S_c is a mass source term per unit volume which accounts for the mass transfer across the boundary due to phase change process. This term is realized by

$$S_c=\frac{\dot{m}_{lv}}{v_e} \tag{6}$$

where $\dot{m}_{lv}$ is the mass flow rate across the liquid-vapour interface and v_e the size of the control volume. For present study, $\dot{m}_{lv}$ was determined by the phase change model which is described in section 3.2. For homogenous multiphase model, the momentum equation is defined by:

$$\frac{\partial(\rho U)}{\partial t}+\nabla\cdot(\rho U\cdot U)=-\nabla p+\nabla\cdot\left[(\mu+\mu_t)(\nabla U+(\nabla U)^T)\right]+\rho g+S_m \tag{7}$$

where p is the pressure, g is the gravity acceleration, and μ is the bulk viscosity which can be obtained by:

$$\mu=\mu_v r_v+\mu_l(1-r_v) \tag{8}$$

where μ_v and μ_l are dynamic viscosities of vapour and liquid. The term μ_t is the eddy (turbulence) viscosity that can be determined using the κ-ω turbulence model [22]. S_m is the momentum source term which stands for the force to the volume ratio due to surface tension effect. This term is computed depends on the model of the continuum surface force [23] as follows:

$$S_m=f_{lv}\delta_{lv} \tag{9}$$

where

$$f_{lv}=-\sigma\,\kappa_{lv}n_{lv}+\nabla\sigma \tag{10}$$

The delta function δ_{lv} and the surface curvature κ_{lv} are expressed by:

$$\delta_{lv}=|\nabla\cdot r_{lv}| \tag{11}$$

and

$$\kappa_{lv}=\nabla\cdot n_{lv} \tag{12}$$

where σ is the coefficient of the surface tension and n_{lv} is the normal vector directed from liquid phase to vapour phase which can be realized by specifying the solid wall-liquid contact angle θ between as follows:

$$n_{lv}=n_w\cos\theta+t_w\sin\theta \tag{13}$$

where n_w and t_w are unit vectors which are directed vertical and tangential to the wall. For the present study, θ was equal to 95° for water [24]. The boiling process involves heat transport inform of sensible and latent heat exchange due to temperature difference between channel walls and inlet water. First, hot channel walls exchange heat energy with liquid water sensibly until the liquid becomes saturated and tiny vapour bubbles appear. Then, the boiling process develops to the condition where the phase change mode will be dominant. Accordingly, the thermal energy conservation equation is defined as:

$$\frac{\partial(\rho H)}{\partial t}+\nabla\cdot(\rho UH)=\nabla\cdot(\lambda\,\nabla T)+S_E \tag{14}$$

where H and λ are the phase enthalpy and thermal conductivity which are specified according to the phase under consideration. The energy equation was solved separately for each phase. The term S_E is the energy source term which accounts for the heat transfer rate during phase change process. Thus,

$$S_E=S_c\,H_{lv} \tag{15}$$

where H_{lv} is the vapourisation latent heat.

3. CFD MODEL DESCRIPTION

In the present research, ANSYS-CFX 15.0 software was adopted for simulating water boiling process through a microchannel. Both solid and fluid domains are taken into accounts. In the CFD model, the channel walls and base

were represented by solid domain while the fluid domain can contain liquid phase or both liquid and vapour phases. A uniform heat flux was subjected to the bottom surface of the microchannel as heat source. The applied heat flux is absorbed by the flowing water through the channel causing to change it from liquid phase to vapour phase. The inlet water temperature was varied to simulate the impact of the subcooling inlet on the flow boiling process. Moreover, heat flux and mass velocity are varied during the simulation to study their effects on the flow boiling behaviour and the corresponding average HTC. Furthermore, the flow patterns for the boiling process is monitored to capture the creation and development of bubbles for each run. The following assumptions are considered for the present simulation:

- Constant thermophysical properties
- The vapour phase is kept at saturation temperature (has negligible thermal resistance).
- Two dimensional simulation.
- The flow is Newtonian and incompressible.
- Transient simulation was considered.

3.1.Model's geometry and boundary conditions

Experimental results were chosen to validate the numerical model of the present work. Jayaramu et al. [24] discussed the influence of different surface roughness of the inner surface of the microchannel. The dimensions of the microchannel were 0.5mm for width, 0.24mm for height and 40mm for length. The experiments were conducted with the following mass velocities (1120 $kg \cdot m^{-2} \cdot s^{-1}$, 1667 $kg \cdot m^{-2} \cdot s^{-1}$ and 2220 $kg \cdot m^{-2} \cdot s^{-1}$) with the heat fluxes 200 $kW \cdot m^{-2}$ to 1200 $kW \cdot m^{-2}$ and for the liquid temperature inlet is 95 ^{o}C.

Solving phase change problem consumes extremely high calculations cost even for small scale models. Thus, in this study, the actual 3D channel was approximated to 2D model with a very thin thickness of 0.005 mm as the ANSYS-CFX can only handle three dimensional models, see Figure 1. For this approximation, the heating source will be supplied from the bottom surface only. In actual rectangular channels, heating is supplied not only from the base wall but also from side walls. ANSYS-ICEM software was used to build the geometry of the model. It consists of three regions: solid (40mm ×0.5mm), mixture (40mm ×0.24mm) and outlet region (20mm×0.24 mm). The solid region was included in the modelling to simulate the conduction heat transfer across channel walls. The base wall thickness was assumed to be 0.5 mm to reduce calculation cost. In the liquid-vapour mixture region, the boiling process is taken place. Therefore, a consideration of a fine mesh near the wall was made to capture the onset nucleate boiling, see Figure 2. The outlet region was integrated to the model to enhance numerical calculation stability as this region can eliminate the effect of reverse flow that may occur at the outlet.

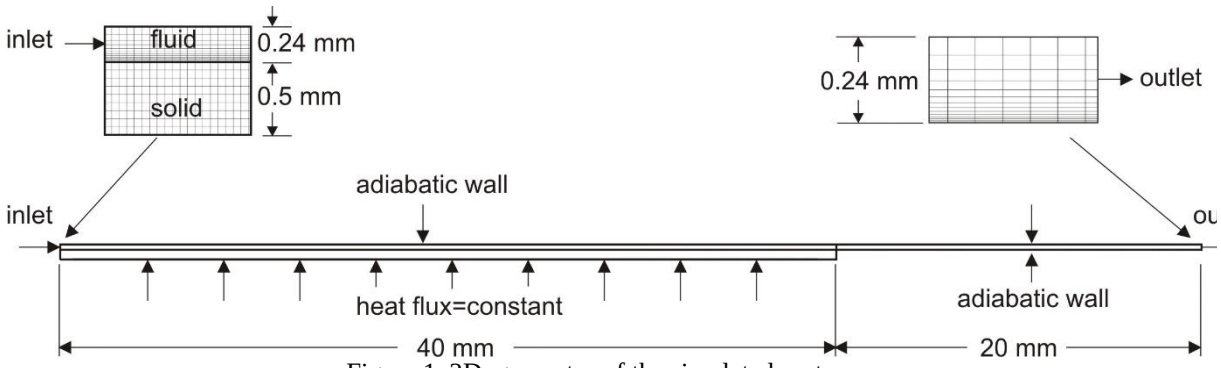

Figure 1. 2D geometry of the simulated system.

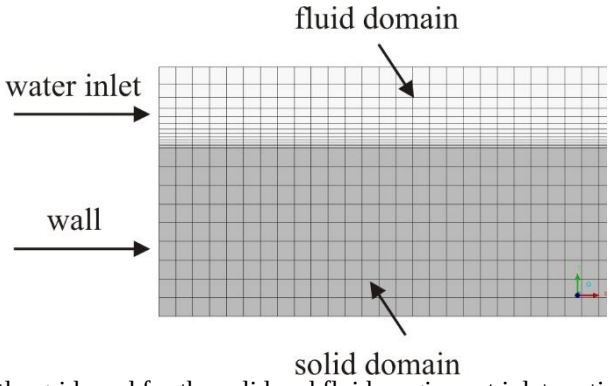

Figure 2. A comparison of the grid used for the solid and fluids regions at inlet section.

The heat flux is supplied at the bottom surface of the solid region as shown in Figure 1. Heat is transferred through the solid wall to the interface which is generated by the numerical model between solid and mixture where the boiling is occurred near the wall. At the inlet, velocity of liquid is given while the outlet is considered to be an "opening" rather than "outlet" according to ANSYS-CFX setting. This setting can take the reverse flow into account. The time step was chosen to be 5×10^{-6} second to ensure calculation stability for the numerical solution and to reach residuals less than 0.001 in key variables of the governing equations.

3.2.Phase change modelling

Conjugate heat transfer between solid and the mixture was modeled to solve energy and momentum equations for the determination of energy transfer and temperature distribution through solid and mixture domain. The thermal phase change model embedded in ANSYS-CFX was utilized to solve the interface between the vapour's phase and liquid's phase in conjunction with the thermal resistance model. The thermal resistance model considered a more general model in which a separate heat transfer coefficients for each phase in order to achieve a heat transfer separately for each phase [21]. According to this model, the sensible heat transfer of the vapour phase q_v is

$$q_v=h_v(T_i-T_v) \tag{16}$$

and the sensible heat transfer of the liquid's phase q_l is expressed by:

$$q_l=h_l(T_i-T_l) \tag{17}$$

where h_v, h_l, T_i, T_v, and T_l are convective HTC of the vapour phase, convective HTC of the liquid phase, interfacial temperature, temperature of the vapour phase, and temperature of the liquid phase, respectively. If there is no mass transfer, the interfacial temperature T_i is determined by the following heat balance

$$q_v+q_l=0 \tag{18}$$

If the mass between the two phases transfers, the interfacial temperature T_i is presumed to equal to T_{sat}. When boiling process starts and an amount of liquid transforms into vapour, i.e. phase change occurs, the total heat transfer energy for both phases Q_v and Q_l can be described by:

$$Q_v=q_v+\dot{m}_{lv}H_v \tag{19}$$

and

$$Q_l=q_l-\dot{m}_{lv}H_l \tag{20}$$

where H_v and H_l are interfacial enthalpies for both phases. The interfacial mass flow rate $\dot{m}_{lv}$ is determined by the heat balance as:

$$Q_v + Q_l = 0 \tag{21}$$

and

$$\dot{m}_{lv}=\frac{q_v+q_l}{H_l-H_v} \tag{22}$$

The nucleation of water starts when the wall temperature increases to a level larger than saturation temperature of the liquid. Boiling starts in tiny and micro cavities present on the heated surface. The calculations continue until steady state occur with residuals less than 0.001 for convergence in key parameters. The the model of wall boiling [21] was considered to simulate transient boiling inside the channel. The liquid and vapour phases were considered as incessant and sparsed phases where the gravity effect was activated. The thermal phase change model with saturation temperature of 100^{o}C was utilized. The Rensselaer Polytechnic Institute (RPI) model [25] was activated which contains several sub-models to precisely predict the onset and the growth of the nucleate boiling. With the help of the RPI model, temperature distribution on channel walls can be realized. This model is based on number of sub-models and engineering correlations. The mechanism of RPI model is used to divide the heated wall length into convective, boiling, and liquid quenching sub regions. In the convective sub region, heat is transferred by convection only and no boiling available. The HTC for this region is determined by Egorov and Menter [26]. For the second sub region, boiling near the heated wall occur. In the third sub region, the liquid carry superheated and saturated vapour leading to a rise in the liquid's temperature (liquid quenching). The liquid quenching HTC is determined according to [27]. Therefore, the total wall rate of heat transfer Q_w can be determined by:

$$Q_w = Q_c + Q_e + Q_q \tag{23}$$

where Q_c, Q_e, and Q_q are convective, evaporation, and quenching heat transfer rates respectively. Q_c can be determined in terms of the convective heat transfer area A_c, convective HTC h_c, wall temperature T_w, and the liquid inlet temperature $T_{l,i}$ as follows:

$$Q_c = A_c h_c (T_w - T_{l,i}) \tag{24}$$

where h_c is determined by turbulence wall function [26]. The evapouration heat transfer rate Q_e is defined as:

$$Q_e = \dot{m}_{lv} H_{lv} \tag{25}$$

and

$$Q_q = A_q h_q (T_w - T_l) \tag{26}$$

where A_q is the liquid quenching area, h_q is the HTC of quenching according to formula of Del Valle and Kenning [27]. The area partitions A_c, A_e, and A_q were determined according to the procedure of RPI model [26]. Bubble detaching diameter was determined depending of the model of Tolubinski and Kostanchuk [28] and the wall nucleation cite density according to Lemmert and Chawla [29] which was later modified by Egorov and Menter [26]. The average HTC ($\bar{h}$) of the flow boiling can be determined by

$$\bar{h} = \frac{q_{flux}}{\bar{T}_w - T_{sat}} \tag{27}$$

where q_{flux} is the applied heat flux and $\bar{T}_w$ is the average wall temperature along the channel. The boiling HTC $\bar{h}_b$ was determined as:

$$\bar{h}_b = \frac{q_{flux}}{\bar{T}_{wb} - T_{sat}} \tag{28}$$

where $\bar{T}_{wb}$ is the average wall temperature for the saturation region only.

4. MESH DEPENDENCY TEST AND MODEL VALIDATION

Mesh dependency exam was performed to achieve a numerical solution stabilization. The number of the longitudinal mesh cells was increased while keeping the cell thickness near the wall constant and equals to 3 μm. The mesh dependency test was achieved by comparing the numerical results of the base wall temperature for four different number of mesh elements, see Figure 3. Four meshing methods with total number of elements equals to 42129, 63129, 84129, and 105129 were tested. Figure 3 showed that that difference in channel wall temperature between the number of mesh elements 84129 and 105129 was 1.5%. Therefore, for time saving the number of mesh elements 84129 was chosen. Accordingly, the maximum cell size was determined to be 50 μm.

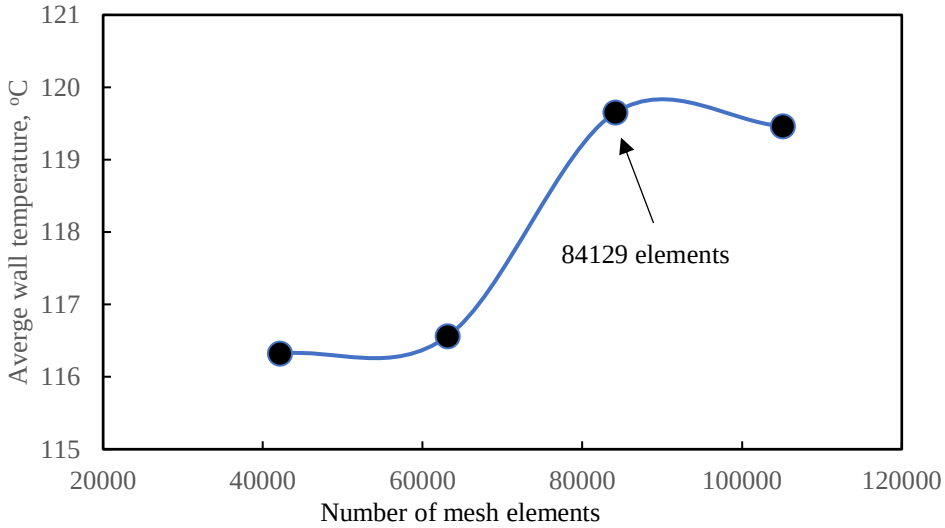

Figure 3. CFD mesh dependency test of the channel lower surface temperature along the channel axis for 42129, 63129, 84129, and 105129 elements mesh.

5. CFD MODEL VALIDATION

The present simulation model results was compared with the experimental results of Jayaramu et.al. [24] to validate the numerical simulation model. The validation was achieved by comparing the boiling HTC of the simulation results using Eq.(28) with that of the experimental work. Figure 4 shows that the experimental boiling HTC on the x-axis versus the predicted one of the simulation model on the y-axis for mass velocity of 1667 $kg \cdot m^{-2} \cdot s^{-1}$ and variable heat flux. The simulation model underpredicted most of data because the 2D model ignored the effect of the channel corners which can trigger the boiling process due the heat concentration. The absolute average deviation of the predicted data was 15.8% compared to the experimental HTC.

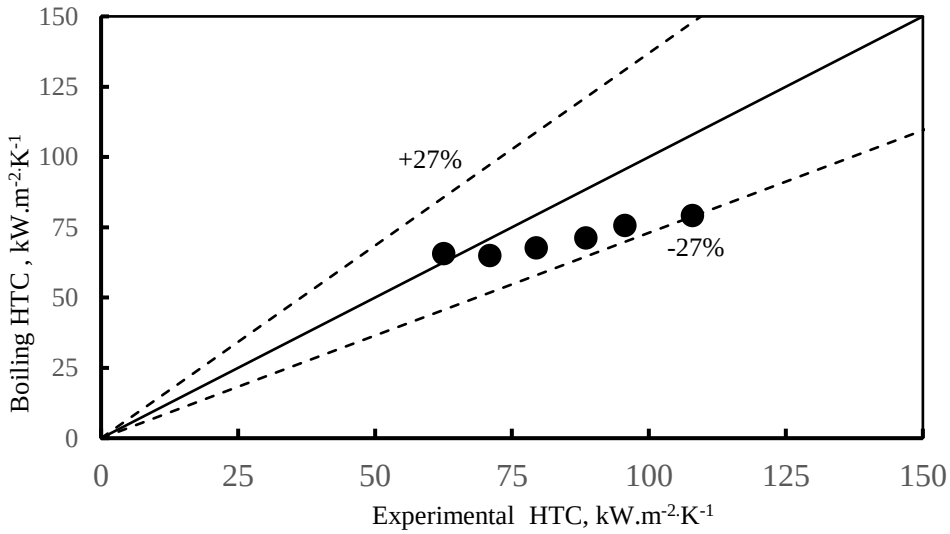

Figure 4. The comparison of HTC of flow boiling for both numerical and experimental results [24].

6. RESULTS

The following results show the variation of flow patterns and bottom wall temperature with channel length for different inlet water temperature (degree of the subcooling), mass velocity, and heat flux. Furthermore, the effect of degree of subcooling on the average HTC of water flow boiling through the microchannel is explored.

6.1.Flow patterns and wall temperature

Figure 5 shows the contours of vapour and liquid volume fractions variation with the inlet water subcooling and heat flux supplied at mass velocity of 400 $kg \cdot m^{-2} \cdot s^{-1}$. The subcooling degree was varied by 5ºC, 10ºC, 15ºC, 20ºC, and 25ºC while the heat flux was varied by 500 $kW \cdot m^{-2}$, 1000 $kW \cdot m^{-2}$ and 1500 $kW \cdot m^{-2}$. These values were chosen to cover a wide range of heat flux to study the effect of lower mass velocity 400 $kg \cdot m^{-2} \cdot s^{-1}$ and higher mass velocity 800 $kg \cdot m^{-2} \cdot s^{-1}$ out of the range of experimental results of Jayaramu et.al. [24]. Vapour and liquid phases are represented by red and blue colors. For heat flux of 500 $kW \cdot m^{-2}$, it can be shown that the boiling process starts early at zero inlet subcooling, see Figure 5a. For the subcooling inlet, the boiling process develops gradually. First, small size bubbles are created near the wall due to the nucleate boiling, and then these bubbles coalescence to form longitudinal bubbles. Finally, the bubbles continue to develop and form slug-wavy flow pattern as seen in Figure 5a. At this stage, the convective boiling will be dominant along the channel. Whereas, for the applied heat fluxes of 1000 $kW \cdot m^{-2}$and 1500 $kW \cdot m^{-2}$, the nucleation of bubbles and the slug-wavy flow patterns develop early, see Figure 5b and Figure 5c.

The change in flow pattern from nucleation to convective boiling is reflected by wall temperature distribution for the mass velocity of 400 $kg \cdot m^{-2} \cdot s^{-1}$ and heat fluxes 500 $kW \cdot m^{-2}$, 1000 $kW \cdot m^{-2}$, and 1500 $kW \cdot m^{-2}$ as shown in Figure 6. The x-axis is the channel length and the y-axis shows the wall temperature.

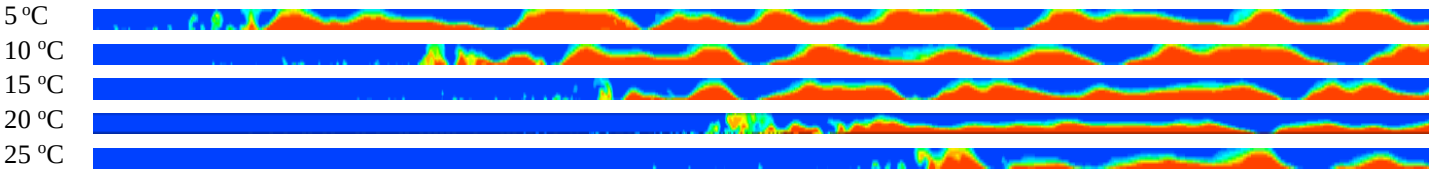

(a) q=500 kW·m^{-2}

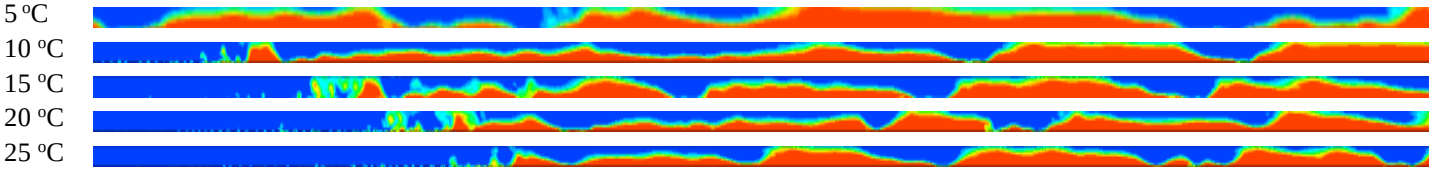

(a) q=1000 kW·m^{-2}

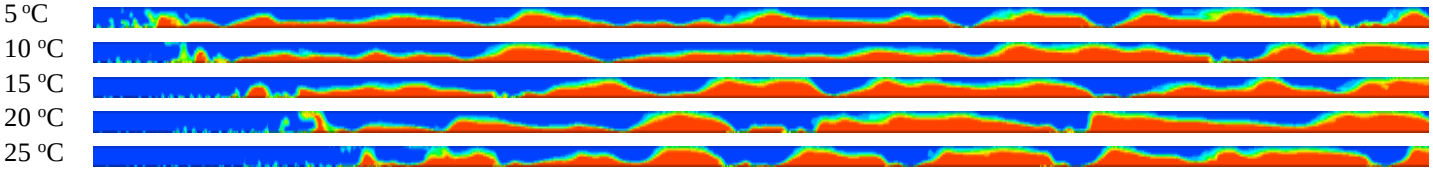

(b) q=1500 kW·m^{-2}

Figure 5. The change in the vapour volume fraction over the axial direction of the channel for the mass velocity 400 kg·m·$^{-2}$s^{-1} and variable heat flux.

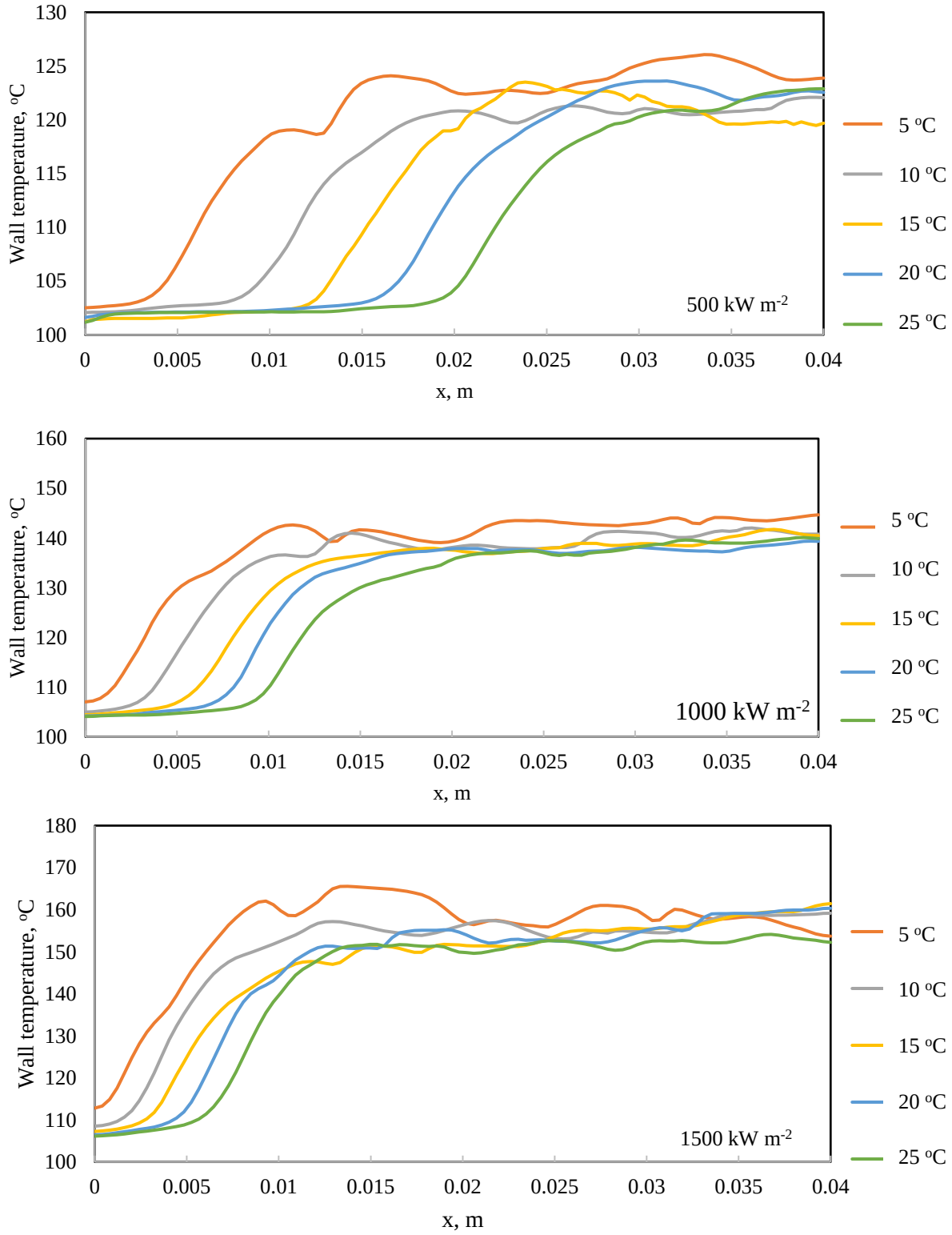

Figure 6. Wall temperature distribution of the subcooling degrees and heat fluxes for the mass velocity 400 kg·m·$^{-2}$s^{-1}.

The bottom wall temperature is evaluated by the CFX simulation of the model at 0.5mm wall thickness with heat flux supplied from the bottom, see section 4. For all data, the wall temperature increases gradually until reaching steady state value with small fluctuation, see Figure 6. The rise in the inlet subcooling led to a decrease in wall temperature, thus the minimum wall temperature was seen with 25 °C degree of subcooling. At the channel entrance, the fluid temperature is low due subcooling and there is a convective single-phase heat transfer mode which has

lower HTC compared to phase change mode. This implies that the wall temperature will be the lowest at the inlet. During the single phase region, water temperature starts to increase gradually until reaching the saturation temperature. After this region, the nucleate boiling starts causing the wall temperature to keep constant as shown in Figure 6. The nucleate boiling continues until longitudinal bubbles appears and the boiling turns into convective boiling. Consequently, the wall temperature rises because of the accumulation of vapour at the channel wall that resulted in an additional thermal resistance. This rise in the wall temperature leads to a significant reduction in local HTC due to of the increase in the difference between liquid bulk saturation temperature and wall temperatures. For the case of 1500 $kW \cdot m^{-2}$, different behaviour can be seen due to numerical calculation instability as the mass flow rate is minimum and heat flux is maximum. Moreover, for the lower heat flux 500 $kW \cdot m^{-2}$ and 400 $kg \cdot m^{-2} \cdot s^{-1}$ Figure 6a, the starting of the boiling is delayed and the sharp increase in the bottom wall temperature is happening earlier for the lower subcooling inlet 5^{o}C. Furthermore, the effect of higher mass velocity 800 $kg \cdot m^{-2} \cdot s^{-1}$ is discussed in the next paragraph.
The results of vapour and liquid volume fractions at mass velocity of 800 $kg \cdot m^{-2} \cdot s^{-1}$ is presented in Figure 7 for the three heat fluxes and the same inlet degrees of subcooling. It is obvious that the development of the nucleate boiling is slower than that of 400 $kg \cdot m^{-2} \cdot s^{-1}$. Moreover, for mass velocity 800 $kg \cdot m^{-2} \cdot s^{-1}$ and heat flux of 500 $kW \cdot m^{-2}$ with subcooling degree 25 ^{o}C, the nucleate boiling is predominant while the forced convective boiling is apparently not existing. This can be confirmed with reference to the Figure 8 where the wall temperature is almost uniform to the outlet of the channel for the case of mass velocity 800 $kg \cdot m^{-2} \cdot s^{-1}$ and heat flux of 500 $kW \cdot m^{-2}$. Thus, it is expected that the local HTC is maximum at this condition.

Figure 9 shows the influence of mass velocity variation with heat flux 1500 $kW \cdot m^{-2}$ and subcooling at the channel inlet for heat flux 500 $kW \cdot m^{-2}$ on the starting of nucleate boiling. Figure 9a demonstrates the nucleation of water bubbles at inlet section of the channel with inlet subcooling 15°C and supplied heat flux 1500 $kW \cdot m^{-2}$ for mass velocities 400 $kg \cdot m^{-2} \cdot s^{-1}$ and 800 $kg \cdot m^{-2} \cdot s^{-1}$. Figure 9b presented the impact of increasing the inlet subcooling (ΔT_i) on the nucleate boiling at fixed mass velocity and heat flux. Figure 9a showed that at the inlet to the channel, the bubble size was developed faster with mass velocity of 400 $kg \cdot m^{-2} \cdot s^{-1}$ as compared to 800 $kg \cdot m^{-2} \cdot s^{-1}$. Because of lower mass velocity means lower flow velocity which leads slower heat transfer rate and lower HTC. Therefore, the boiling will start earlier for 400 $kg \cdot m^{-2} \cdot s^{-1}$. Moreover, the nucleate boiling was delayed when the inlet subcooling become larger with fixed mass velocity and heat flux, see Figure 9b.

In summary, the wall temperature starts with low value and then increase sharply. The channel length of low wall temperature depends on the inlet subcooling degree. The subcoooling length can be classified into two regions, first region where the single phase heat transfer mechanism is taking place. The second, the HTC increases due to the start of nucleate boiling [18]. Then, the HTC starts to drop due to the transfer of the flow to slug flow pattern where the convective boiling occurs. The rise in supplied heat flux is going to shorten the subcooling length and extend the convective boiling region, see Figure 6 and Figure 8.

6.2. Average HTC

Figure 10 and **Error! Reference source not found.** demonstrate the change in the average HTC with subcooling degree for various heat flux (500 $kW \cdot m^{-2}$, 1000 $kW \cdot m^{-2}$ and 1500 $kW \cdot m^{-2}$) and mass velocity (400 $kg \cdot m^{-2} \cdot s^{-1}$ and 800 $kg \cdot m^{-2} \cdot s^{-1}$). The x- axis represents the inlet subcooling while the y-axis axis shows the average HTC of the flow boiling through the channel. The average HTC is determined by the average wall temperature from Eq.(26). For both figures, it can be shown that the average HTC raises with the increase in the subcooling. These figures show two different regions separated by a reflection point.
At the low subcooling degree (before the reflection point), the highest value of heat flux gives the maximum value of the average HTC, see Figure 10 and **Error! Reference source not found.**. After the reflection point, the lowest heat flux gives the maximum average HTC. Figure 10 shows that the reflection point for the mass velocity of 400 $kg \cdot m^{-2} \cdot s^{-1}$ occurs at 7 ^{o}C subcooling while **Error! Reference source not found.** shows that the reflection occurs a pproximately at 5 ^{o}C.
The existence of the reflection point may be explained by equal values of the average HTC with various heat fluxes. Figure 10 and **Error! Reference source not found.** showed that for a specific mass velocity and different heat fluxes, the average HTC will be the same for the degree of subcooling at reflection point.
Error! Reference source not found. shows that for heat flux of 500 $kW \cdot m^{-2}$ and mass velocity of 800 $kg \cdot m^{-2} \cdot s^{-1}$, t here is a sharp jump in the average HTC after subcooling degree of 20 ^{o}C. This can be justified by Figure 7 where for the degrees of subcooling 20 ^{o}C and 25 ^{o}C, the nucleate boiling was predominant to the end of the channel.
According to above, it can be noted that the impact of the heat flux on the average HTC is dependent on the degree of subcooling. This effect is more pronounced before the reflection point for mass velocity of 400 $kg \cdot m^{-2} \cdot s^{-1}$ as compared to that of the mass velocity 800 $kg \cdot m^{-2} \cdot s^{-1}$.

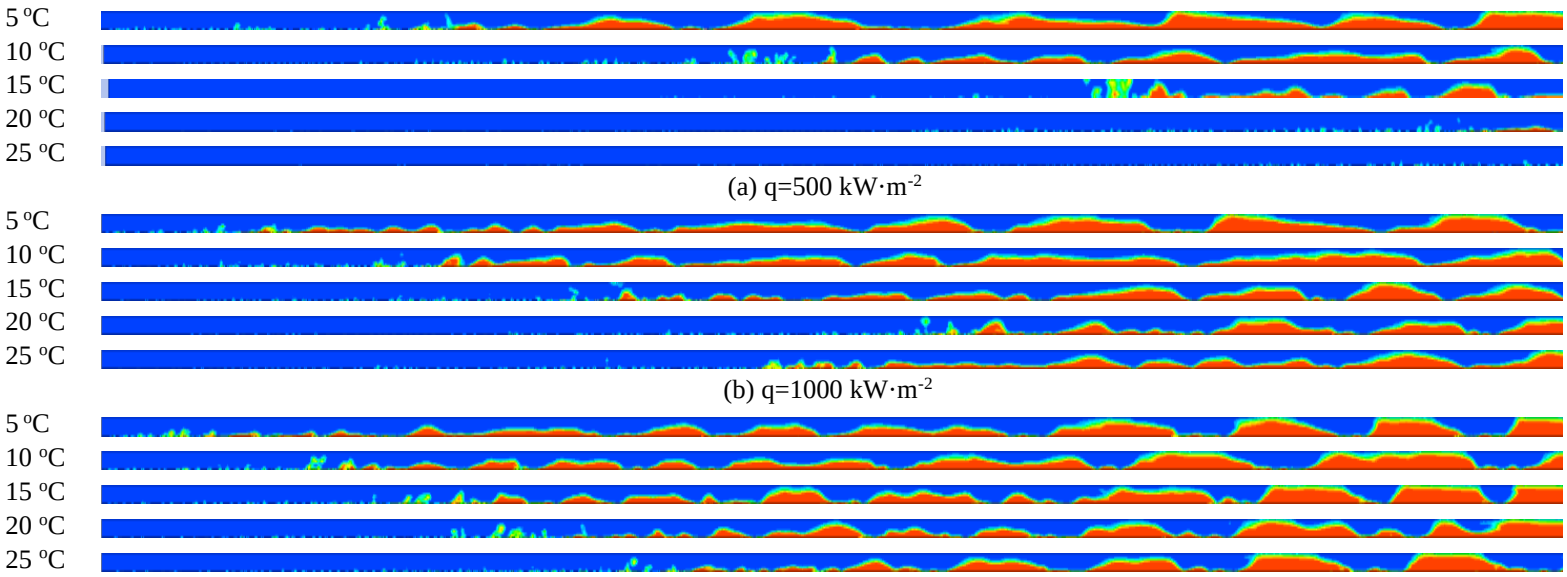

(a) q=500 kW·m^{-2}

(b) q=1000 kW·m^{-2}

(c) q=1500 kW·m^{-2}

Figure 7. The change in the vapour volume fraction along the axial direction of the channel for the mass velocity 800 kg·m·$^{-2}$s^{-1} and different heat flux.

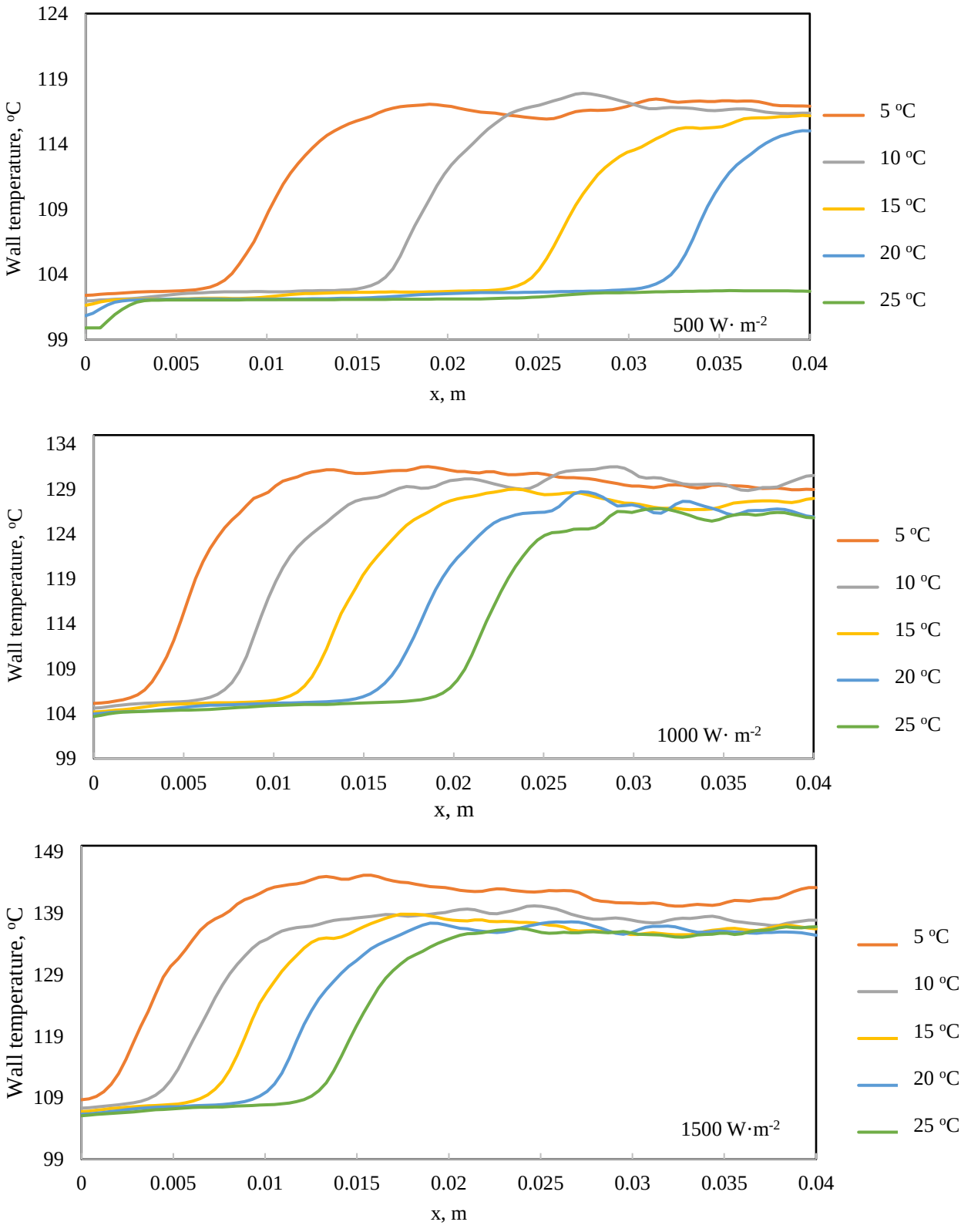

Figure 8. Wall temperature distribution of the subcooling degrees and heat fluxes for the mass velocity 800 kg·m·$^{-2}$s^{-1}.

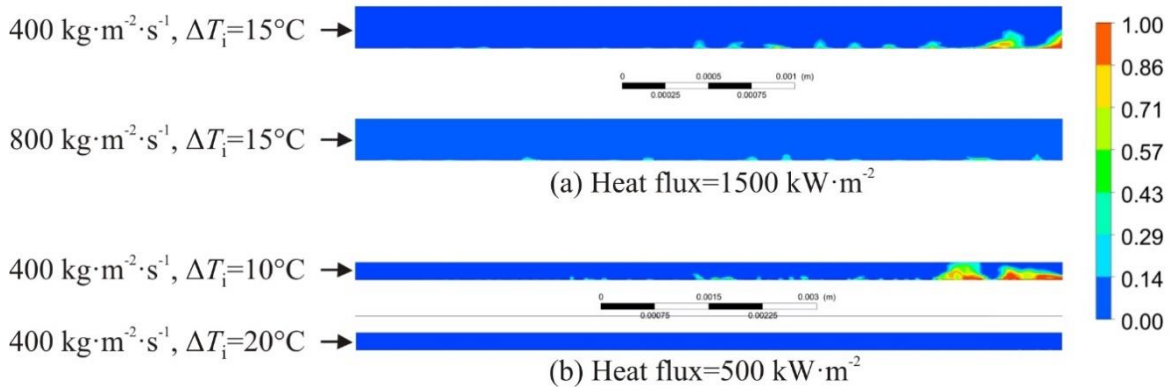

Figure 9. Vapour volume fraction with respect to (a)variable mass velocity and (b) inlet subcooling ΔT_i.

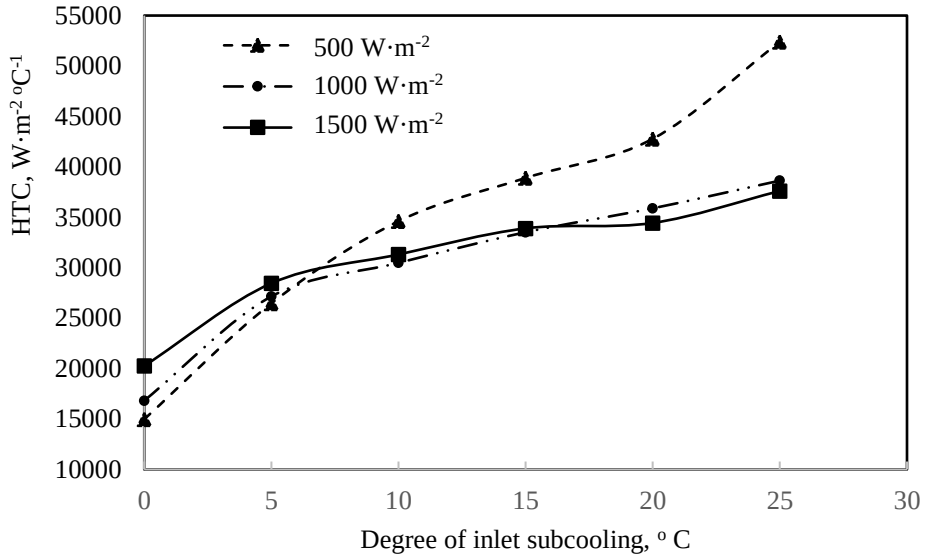

Figure 10. Variation of the average HTC with different subcooling degree and different heat fluxes for the mass velocity 400 kg·m·$^{-2}$s^{-1}.

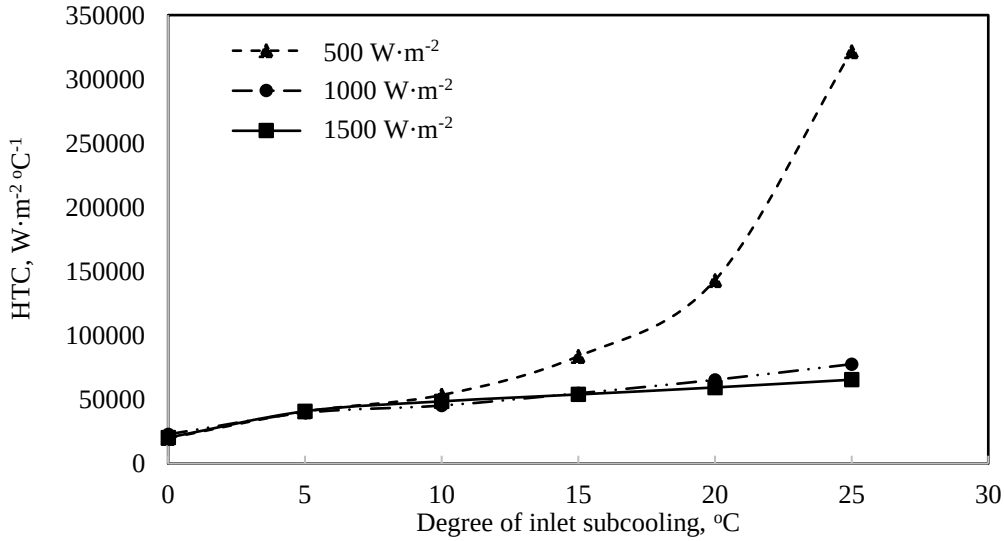

Figure 11. Variation of the average HTC with different subcooling degree and different heat fluxes for the mass velocity 800 kg·m·$^{-2}$s^{-1}.

7. Conclusions

In the present work, CFD simulation of water flow boiling inside a microchannel with 0.24 mm deep and 40 mm length was performed. Inlet water temperature was changed so that the degree of subcooling varied by 5 ºC, 10 ºC, 15 ºC, 20 ºC, and 25 ºC. Heat flux was changed by 500 kW·m^{-2}, 1000 kW·m^{-2}, and 1500 W·m^{-2} and mass velocity was changed by 400 kg·m·$^{-2}$s^{-1} and 800 kg·m·$^{-2}$s^{-1}.

It can be concluded that the two dimensional CFD simulation can predict wall temperature variation during flow boiling with acceptable accuracy. The degree of subcooling of the inlet liquid has a considerable effect on both the wall temperature of the channel and boiling flow patterns. The rise in the subcooling degree kept nucleate boiling flow and delayed the development of convective boiling. However, for a specific channel geometry, this effect is highly counted on the heat flux and mass velocity. The average HTC enhances with the rise in the degree of inlet subcooling. The increase in heat flux may rise or reduce the average HTC relying on the position of the reflection point. Thus, the degree of subcooling and the heat flux should be simultaneously considered when it comes to enhancement of HTC during boiling inside microchannel. It was shown from Figure 10, mass velocity 400 kg·m·$^{-2}$s^{-1}, HTC increases by 35% for heat fluxes 500 kW·m^{-2} and 1000 kW·m^{-2} for subcooling inlet 25ºC as compared to 5ºC. While for the same mass velocity the increase in HTC was 89% for ^{2} for subcooling inlet 25ºC as compared to 5ºC. It was shown from Figure 11, mass velocity 800 kg·m·$^{-2}$s^{-1}, HTC increases by 62% for heat fluxes 500 kW·m^{-2} and 1000 kW·m^{-2} for subcooling inlet 25ºC as compared to 5ºC. While for the same mass velocity the increase in HTC was 700% for ^{2} for subcooling inlet 25ºC as compared to 5ºC.

Nomenclature

Symbol	Definition	Unit
A	Area	[m^2]
g	Gravitational acceleration	[m^2·s^{-1}]
h	Convective heat transfer coefficient	[kJ·m^{-2} ºC^{-1}]
H	Enthalpy	[kJ·kg^{-1}]
$\dot{m}$	Mass flow rate	[kg·s^{-1}]
p	Pressure	[Pa]
Q	Heat transfer rate	[W]
q	Sensible heat flux	[W·m^{-2}]
r	volume fraction	[ºC]
$\bar{T}$	Average temperature	[ºC]
t	Time	[s]
U	Velocity	[m·s^{-1}]
v_e	Control volume element	m^3

Greek letter

Symbol	Definition	Unit
ρ	Density or Bulk density	[kg·m^{-3}]
λ	Thermal conductivity	[kJ·m^{-1} ºC^{-1}]
μ	Dynamic viscosity	[kg· m^{-1} ·s^{-1}]
σ	surface tension coefficient	N. m^{-1}

Subscript

b	boiling
c	convective
e	evaporation
lv	Liquid to vapour
i	Interfacial, inlet
l	liquid
q	quenching
s	solid
sat	saturation
v	vapour
w	wall

Abbreviations

3D Three dimensional

CFD Computational fluid dynamics

CHF Critical heat flux

HTC Heat transfer coefficient

FDB Fully developed boiling

ONB Onset of nucleate boiling

OAS Onset of accelerated sliding

PDB Partially developed boiling

RPI Rensselaer Polytechnic Institute

REFERENCE

[1] D. B. Tuckerman and R. F. W. Pease, "High-performance heat sinking for VLSI," *IEEE Electron Device Lett.*, vol. 2, no. 5, pp. 126–129, May 1981, doi: 10.1109/EDL.1981.25367.

[2] W. Qu and I. Mudawar, "Flow boiling heat transfer in two-phase micro-channel heat sinks—I. Experimental investigation and assessment of correlation methods," *International Journal of Heat and Mass Transfer*, vol. 46, no. 15, pp. 2755–2771, Jul. 2003, doi: 10.1016/S0017-9310(03)00041-3.

[3] W. Qu and I. Mudawar, "Flow boiling heat transfer in two-phase micro-channel heat sinks—II. Annular two-phase flow model," *International Journal of Heat and Mass Transfer*, vol. 46, no. 15, pp. 2773–2784, Jul. 2003, doi: 10.1016/S0017-9310(03)00042-5.

[4] J. D. Schwarzkopf, S. G. Penoncello, and P. Dutta, "Enhanced boiling heat transfer in mesochannels," *International Journal of Heat and Mass Transfer*, vol. 52, no. 25–26, pp. 5802–5813, Dec. 2009, doi: 10.1016/j.ijheatmasstransfer.2009.07.022.

[5] S. Szczukiewicz, N. Borhani, and J. R. Thome, "Fine-resolution two-phase flow heat transfer coefficient measurements of refrigerants in multi-microchannel evaporators," *International Journal of Heat and Mass Transfer*, p. 17, 2013, doi: https://doi.org/10.1016/j.ijheatmasstransfer.2013.08.078.

[6] L. Cheng and G. Xia, "Fundamental issues, mechanisms and models of flow boiling heat transfer in microscale channels," *International Journal of Heat and Mass Transfer*, vol. 108, pp. 97–127, May 2017, doi: 10.1016/j.ijheatmasstransfer.2016.12.003.

[7] P. K. Das and A. K. Das, "Instability in Flow Boiling through Microchannels," in *Microchannel Phase Change Transport Phenomena*, Elsevier, 2016, pp. 257–286. doi: 10.1016/B978-0-12-804318-9.00007-8.

[8] J. Lee and I. Mudawar, "Critical heat flux for subcooled flow boiling in micro-channel heat sinks," *International Journal of Heat and Mass Transfer*, vol. 52, no. 13–14, pp. 3341–3352, Jun. 2009, doi: 10.1016/j.ijheatmasstransfer.2008.12.019.

[9] R. Ahmadi, A. Nouri-Borujerdi, J. Jafari, and I. Tabatabaei, "Experimental study of onset of subcooled annular flow boiling," *Progress in Nuclear Energy*, vol. 51, no. 2, pp. 361–365, Mar. 2009, doi: 10.1016/j.pnucene.2008.05.003.

[10] J.-M. Le Corre, S.-C. Yao, and C. H. Amon, "Two-phase flow regimes and mechanisms of critical heat flux under subcooled flow boiling conditions," *Nuclear Engineering and Design*, vol. 240, no. 2, pp. 245–251, Feb. 2010, doi: 10.1016/j.nucengdes.2008.12.008.

[11] Y. Sun, L. Zhang, H. Xu, and X. Zhong, "Subcooled flow boiling heat transfer from microporous surfaces in a small channel," *International Journal of Thermal Sciences*, vol. 50, no. 6, pp. 881–889, Jun. 2011, doi: 10.1016/j.ijthermalsci.2011.01.019.

[12] S. Vafaei and D. Wen, "Critical heat flux of nanofluids inside a single microchannel: Experiments and correlations," *Chemical Engineering Research and Design*, vol. 92, no. 11, pp. 2339–2351, Nov. 2014, doi: 10.1016/j.cherd.2014.02.014.

[13] L. Yin, L. Jia, and M. Xu, "Experimental investigation on bubble sliding during subcooled flow boiling in microchannel," *Experimental Thermal and Fluid Science*, vol. 68, pp. 435–441, Nov. 2015, doi: 10.1016/j.expthermflusci.2015.05.010.

[14] L. Yin, R. Xu, P. Jiang, H. Cai, and L. Jia, "Subcooled flow boiling of water in a large aspect ratio microchannel," *International Journal of Heat and Mass Transfer*, vol. 112, pp. 1081–1089, Sep. 2017, doi: 10.1016/j.ijheatmasstransfer.2017.05.028.
[15] S. Lee, V. S. Devahdhanush, and I. Mudawar, "Investigation of subcooled and saturated boiling heat transfer mechanisms, instabilities, and transient flow regime maps for large length-to-diameter ratio micro-channel heat sinks," *International Journal of Heat and Mass Transfer*, vol. 123, pp. 172–191, Aug. 2018, doi: 10.1016/j.ijheatmasstransfer.2018.02.020.
[16] I. Yeo and S. Lee, "2D computational investigation into transport phenomena of subcooled and saturated flow boiling in large length to diameter ratio micro-channel heat sinks," *International Journal of Heat and Mass Transfer*, vol. 183, p. 122128, Feb. 2022, doi: 10.1016/j.ijheatmasstransfer.2021.122128.
[17] J. Lee, L. E. O'Neill, S. Lee, and I. Mudawar, "Experimental and computational investigation on two-phase flow and heat transfer of highly subcooled flow boiling in vertical upflow," *International Journal of Heat and Mass Transfer*, vol. 136, pp. 1199–1216, Jun. 2019, doi: 10.1016/j.ijheatmasstransfer.2019.03.046.
[18] Y.-J. Chen, K. Ling, H. Ding, Y. Wang, S.-Q. Jin, and W.-Q. Tao, "3-D numerical study of subcooled flow boiling in a horizontal rectangular mini-channel by VOSET," *International Journal of Heat and Mass Transfer*, vol. 183, p. 122218, Feb. 2022, doi: 10.1016/j.ijheatmasstransfer.2021.122218.
[19] X. Jiang, S. Zhang, Y. Li, Z. Wang, and C. Pan, "Achieving ultra-high coefficient of performance of two-phase microchannel heat sink with uniform void fraction," *International Journal of Heat and Mass Transfer*, vol. 184, p. 122300, Mar. 2022, doi: 10.1016/j.ijheatmasstransfer.2021.122300.
[20] S. Zhou, X. Xu, and B. G. Sammakia, "Modeling of boiling flow in microchannels for nucleation characteristics and performance optimization," *International Journal of Heat and Mass Transfer*, vol. 64, pp. 706–718, Sep. 2013, doi: 10.1016/j.ijheatmasstransfer.2013.05.031.
[21] ANSYS Inc., *ANSYS CFX 15.0 Theory Guide*. Canonsburg, USA: ANSYS Inc.
[22] F. R. Menter, "Two-equation eddy-viscosity turbulence models for engineering applications," *AIAA Journal*, vol. 32, no. 8, pp. 1598–1605, Aug. 1994, doi: 10.2514/3.12149.
[23] J. U. Brackbill, D. B. Kothe, and C. Zemach, "A Continuum Method for Modelling Surface Tension," vol. 100, no. 2, pp. 335–354, 354, 1992 335AD, doi: https://doi.org/10.1016/0021-9991(92)90240-Y.
[24] P. Jayaramu, S. Gedupudi, and S. K. Das, "Influence of heating surface characteristics on flow boiling in a copper microchannel: Experimental investigation and assessment of correlations," *International Journal of Heat and Mass Transfer*, 2019, doi: https://doi.org/10.1016/j.ijheatmasstransfer.2018.08.075.
[25] N. Kurul and M. Z. Podowski, "On the modeling of multidimensional effects in boiling channels," in *ANS Proc. 27th National Heat Transfer Conference, Minneapolis, MN*, Minneapolis, MN, Jul. 1991. doi: http://dx.doi.org/10.1615/IHTC9.40.
[26] Y. Egorov and F. Menter, "Experimental implementation of the RPI boiling model in CFX-5.6," Technical Report ANSYS TR-04-10, 2004.
[27] V. H. Del Valle and D. B. R. Kenning, "Subcooled flow boiling at high heat flux," vol. 28, p. 1907, 1985, doi: https://doi.org/10.1016/0017-9310(85)90213-3.
[28] V. I. Tolubinski and D. M. Kostanchuk, "Vapour bubbles growth rate and heat transfer intensity at subcooled water boiling," presented at the Forth International Heat Transfer Conference, Paris, France, 1977. doi: http://dx.doi.org/10.1615/IHTC4.250.
[29] M. Lemmert and J. M. Chawla, "Influence of flow velocity on surface boiling heat transfer coefficient," in *Heat Transfer and Boiling*, E. Hahne and U. Grigull., Academic Press, 1977.